Engineering Structures 362 (2026) 122997

Contents lists available at ScienceDirect

Engineering Structures

journal homepage: www.elsevier.com/locate/engstruct

Analytical evaluation of cable corrosion effects on the residual prestressing coactive state in post-tensioned concrete elements

Emma Ghini *, Matteo Marra, Giada Gasparini, Stefano Silvestri

DICAM – Department of Civil, Chemical, Environmental and Materials Engineering, University of Bologna, Viale del Risorgimento 2, Bologna 40136, Italy

ARTICLE INFO

Keywords:
Bridges
Post-tensioning
Bonded tendons
Defective grouting
Corrosion
Prestressing force
Cable stress

ABSTRACT

The paper provides an original analytical evaluation of the effects of cable corrosion on the prestressing coactive state in post-tensioned concrete elements (namely, beams and stays in prestressed bridges), in which steel cables are made adherent through subsequent cast-in-situ grouting. The corrosion is assumed to be homogeneously distributed over a finite portion of the sheathing duct characterized by lack of mortar injection, and modeled as a uniform cross-section loss. The study analytically demonstrates that the reduction of the cross-sectional area of the prestressing steel cables due to corrosion generates both (I) a loss of the prestressing force and (II) a stress redistribution within the residual cross-sectional area of the cables, which are limited to the zone lacking grouting. Ready-to-use closed-form mathematical expressions for these two effects are derived allowing direct quantification of the corrosion-induced variation of the prestressing state, for the two cases of concentric and eccentric tendons, and validated against experimental results available in the scientific literature. A numerical application to three typical existing bridge elements is also provided. The fundamental result is that the loss of the prestressing force is approximately equal to the cross-section loss, while the stress redistribution is comparatively small, providing a cable stress increase below 5% for bridge decks and below 25% for stays, even for highly corroded cables.

1. Introduction

Since the '50s, the post-tensioning technology with subsequent grouting leading to a bonded tendon configuration has represented an effective solution, especially for long-span and cast-in-situ bridges. However, it is prone to corrosion phenomena [1,2]. Corrosion leads to a reduction of the cross-sectional area of the prestressing cables, often limited to the zone characterized by lack of grouting (unbonded tendon zone), which clearly affects the mechanical behavior of the post-tensioned elements, including the peak strength and ductility, both of which are critical at the Ultimate Limit State (ULS) and the residual prestressing force, which is relevant for the structural behavior at the Serviceability Limit State (SLS).

On one hand, the effects of the reduction of the cross-sectional area of wires and strands on their axial force capacity at ULS have been studied by many researchers [3–11] including some of the present authors [12–14]. In general, the ultimate stress and strain of prestressing cables reduce with the increase of section loss due to corrosion, as proven analytically [15] and experimentally [6,8]. Various empirical models compute the residual flexural capacity of post-tensioned beams at the ultimate condition. For instance, Lu et al. [16] adapted the classical formulation of the ultimate bending moment of a post-tensioned beam accounting for corrosion in terms of reduction of the prestressing steel area, reduction of the prestressing steel yielding strength, and degradation of the bonding performance between the steel and the surrounding concrete. Recupero et al. [17] estimate the ultimate flexural capacity of corroded post-tensioned elements on the basis of the experimental response of a set of damaged specimens tested to 3-point bending. Other studies exploit the implementation of modified stress-strain relationships within detailed Finite Element models [18].

On the other hand, the effects of the reduction of the cross-sectional area of the prestressing cables on the residual prestressing coactive state in the unbonded zone characterized by lack of grouting, at SLS, is still an open scientific issue. Indeed, research works available in the literature only refer to the case of unbonded tendons along the full length of the post-tensioned concrete element [19,20]. In detail, MacDougall and Bartlett derived a mechanical model for unbonded seven-wire tendons with symmetric broken wires [19] and a single (asymmetric) broken

* Corresponding author.
E-mail address: emma.ghini2@unibo.it (E. Ghini).

https://doi.org/10.1016/j.engstruct.2026.122997
Received 16 August 2025; Received in revised form 17 April 2026; Accepted 11 May 2026
Available online 17 May 2026

wire [20], demonstrating that the failure of the wires induces several effects. Among these, two main effects are envisaged: (I) loss of prestressing force and (II) stress redistribution among the residual cables. These aspects represent the core of the present research work. Indeed, besides being critical for SLS verifications (deformability, cracking, …), from a ULS verification point of view, the loss of prestressing force also plays a central role in the evaluation of the ultimate shear capacity of post-tensioned beams, while it has minor effects on the ultimate flexural one. The ultimate shear capacity is investigated by Granata et al. [21] who proposed a methodology for safety checks through a bending moment–shear force interaction domain in ultimate conditions with axial force due to both prestressing and external loads. However, the formulation of an analytical model describing the residual coactive state for post-tensioned elements with deficient grouting when subjected to corrosion is still to be developed, and it is instrumental to assess the actual condition of post-tensioned bridges. To contribute in this direction, the present work proposes and validates modification factors (a prestressing force ratio and a cable stress ratio) that quantify the corrosion-induced alteration of the coactive state. These factors are directly applicable to the prestressing forces and stresses associated with the uncorroded condition, for both SLS and ULS structural assessments.

2. Problem formulation: assumptions and approach

The problem is formulated considering a post-tensioned concrete element characterized by defective grouting with reference to two physical conditions, represented in Fig. 1: condition before corrosion (Fig. 1a) and condition after corrosion (Fig. 1b).

The following assumptions are made:

- Regarding the cross-section of the structural element, the analyses are carried out under the classical hypotheses: (Assumption #1) plane sections remain plane; (Assumption #2) linear elastic behavior of the materials; (Assumption #3) perfect bonding between concrete and both ordinary and prestressing steel (in bonded zones); (Assumption #4) tensile stresses in the concrete are neglected.
- Regarding the prestressing cables: (Assumption #5) all the cables (i.e. wires, strands or bars, within one or more ducts) are considered as lumped into a single equivalent cable in a single equivalent duct; (Assumption #6) the detailed effects due to the specificity of the arrangement and shape of the cables are neglected (e.g., in case of strands: the contribution due to the lay angle, any kind of frictional interaction between the wires, local stress concentrations that occur due to the irregular shape, etc.).
- Regarding the prestressing force before corrosion: (Assumption #7) the prestressing force is assumed to be uniform along the entire tendon length. Both short-term and long-term prestress losses should be also considered as uniform over the entire length.
- Regarding the corrosion: (Assumption #8) over the entire extent of the zone lacking mortar injection, the prestressing steel is assumed to be completely unbonded with respect to the surrounding concrete and affected by a uniformly distributed corrosion process, leading to a homogeneous reduction of the initial prestressing steel area. Accordingly, corrosion is assumed to be uniform along the considered corroded length. Localized corrosion phenomena (e.g., pitting corrosion), which may induce severe stress concentrations and premature brittle failure, are not addressed in the present formulation and are outside the scope of this study.
- Regarding the interface between unbonded and bonded zones: (Assumption #9) the zones adjacent to the unbonded one are assumed to behave as fully bonded zones providing anchorage through adherence, allowing for variation of the prestressing force.
- Regarding the effects of corrosion, the fundamental assumption (Assumption #10) is that the reduction of the prestressing steel area leads to the following two effects, that occur simultaneously:

(I) a loss of the prestressing force (uniform along the ungrouted length);
(II) a stress redistribution in the residual prestressing steel area.

The approach adopted for the analytical developments consists in the application of the classical principles of structural mechanics, such as congruence and equilibrium, starting from the above-mentioned fundamental assumption regarding the fact that the two effects happen simultaneously. An analytical solution will be found which is at the same time consistent with this initial assumption, as well as both congruent and balanced.

2.1. Condition before corrosion

Fig. 1a provides a schematic representation of a post-tensioned element with defective grouting prior to corrosion initiation. The element is subjected to a prestressing coactive state induced by the prestressing steel cables, lumped in an equivalent cable characterized by

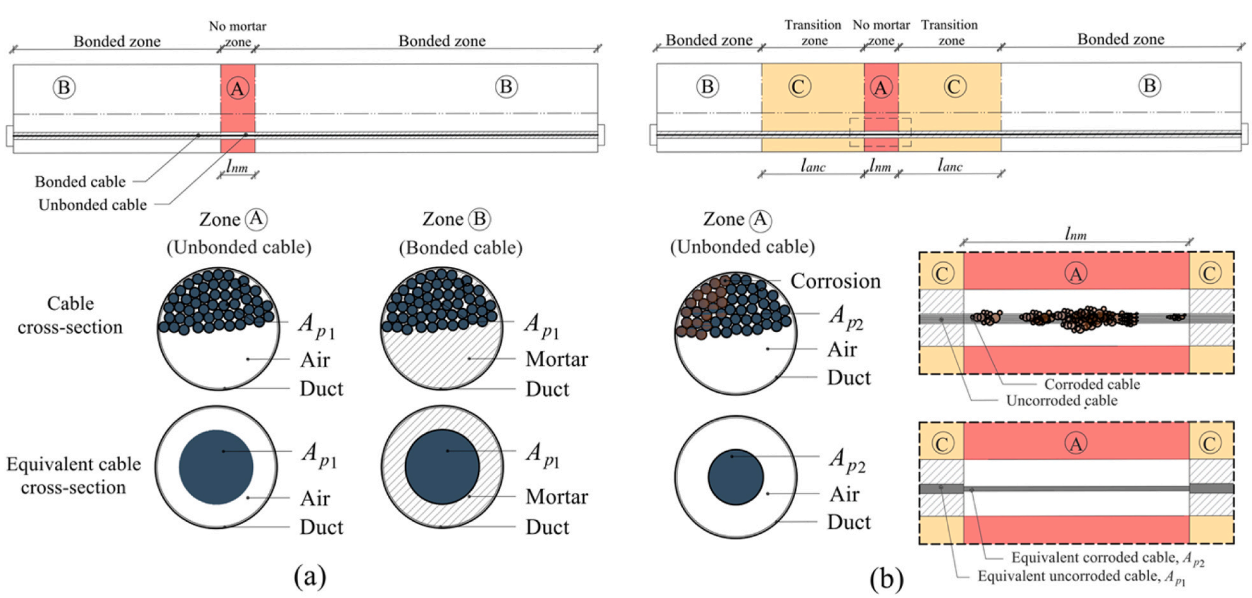

Fig. 1. Post-tensioned element with defective grouting: (a) before corrosion initiation; (b) after corrosion development.

an initial total area equal to A_{p1} and located inside the duct filled with mortar. The portion of the duct where the mortar is not injected correctly is indicated by l_{nm} (no-mortar length). Hence, the interaction between the cable and the surrounding concrete is not uniform throughout the entire extent of the considered element.

In detail, zone A (highlighted in red) identifies the portion of the duct lacking mortar. In this zone, the prestressing steel reinforcement is not effectively adherent to the concrete, due to the fact that inhomogeneous grouting usually generates the presence of air inside the duct, as schematized in the cable cross-section. In this zone, the cable is considered unbonded. On the contrary, due to the presence of mortar in the duct, zone B is characterized by a complete adherence between the two materials (prestressing steel and concrete), therefore the cable is considered uniformly bonded.

The strains inside the materials in zones A and B vary according to the presence of bonding between prestressing steel and concrete. In particular, in zone B, since the cable is homogeneously bonded to the concrete, when the tendon is subjected to an external load or a prestressing force variation, the cross-section integrally reacts with its whole homogenized area. On the contrary, for the same loading condition, in zone A, the strain in the unbonded cable is independent from the surrounding concrete.

2.2. Condition after corrosion

From a structural perspective, the corrosion phenomena substantially modify the existing prestressing steel cables according to three different zones, as graphically schematized in Fig. 1b which also highlights the randomness of the corrosion both in terms of longitudinal and transversal distribution in the unbonded zone (zone A). Typically, for structural purposes, the corrosion-induced modification on the initial amount of prestressing steel is modeled in terms of mass loss [22] or cross-section loss [3–12,16]. In this study, corrosion is modeled as a cross-sectional area reduction which is supposed to be uniformly distributed, both longitudinally (along the whole portion of the sheathing duct which is characterized by lack of mortar injection) and transversally (in terms of reduction of the cross-sectional area of the prestressing cable). The residual (uncorroded) area is identified as A_{p2}.

The modification of the prestressing steel area occurring in the unbonded portion of the cable (zone A) leads to a coactive state variation, which triggers the anchorage functioning of a "transition" zone (zone C). In fact, whenever the prestressing force in zone A changes, the adjacent zones physically act as anchorages that guarantee the bonding of the cable, similar to what happens at the extremities of pre-tensioned non-end-anchored beams, in which the prestressing force is effectively fully transferred from the steel to the concrete after a given anchorage length. Hence, as per what holds for adherent cables, the variation of the prestressing coactive state affects a limited zone, made up of the no-mortar length (l_{nm}) plus a cable anchorage length (l_{anc}) on each side, which is approximately 70–80 times the diameter of the cable [23].

From a theoretical standpoint, the proposed model does not impose strict limits on the no-mortar length, provided it remains smaller than the total tendon length minus twice the anchorage length. This condition is generally met, as realistic values of l_{nm} are typically about 4–5% of the tendon length [24]. The no-mortar region should be positioned to allow such that full anchorage length can develop at both ends, i.e., at a minimum distance l_{anc} from the element ends. Of course, the smaller the actual value of l_{nm}, the higher the representativeness of Assumption #8.

3. Analytical formulation of the residual prestressing coactive state due to corrosion

The analytical developments are presented with reference to a generic cross-section of a post-tensioned element which consists of three materials: concrete, ordinary steel, and high-strength prestressing steel. The elastic moduli of the three materials are indicated with E_c, E_s and E_p, respectively.

The equivalent cable is represented by the total prestressing steel area in two different configurations: (i) the concentric tendon (Fig. 4), and (ii) the eccentric tendon (Fig. 6). The cross-section of the prestressed element is characterized by a concrete net area A_c and by the presence of ordinary reinforcement A_s. As previously introduced, the prestressing steel area, generally indicated as A_p, is identified by A_{p1} and A_{p2} when referring to the tendon condition before and after corrosion, respectively. Then the transformed section that includes concrete and ordinary reinforcement only is computed as $A_{cn} = A_c + n_s A_s$, while the transformed section that includes concrete, ordinary reinforcement, and prestressing steel is computed as $A_{ci} = A_{cn} + n_p A_p$, where the two modular ratios are $n_s = E_s/E_c$ and $n_p = E_p/E_c$. The center of mass and the moment of inertia of the cross-section considering concrete and ordinary reinforcement only are indicated with G_{cn} *and* J_{cn}, respectively. Analogously, the center of mass and the moment of inertia of the cross-section considering concrete, ordinary reinforcement, and prestressing steel are indicated with G_{ci} and J_{ci}, respectively. In the eccentric tendon configuration, e_{cn} represents the cable eccentricity with respect to the center of mass G_{cn}, while e_{ci} represents the cable eccentricity with respect to the center of mass G_{ci}.

3.1. Concentric tendon

A concentric tendon configuration refers to a prestressing tendon whose equivalent cable is located at the centroid of the cross-section, thus inducing a purely axial stress state without bending effects. This configuration typically represents the case of a prestressed stay or tendon working in pure tension. In this case, the ordinary reinforcement is assumed to be symmetrically arranged with respect to the cross-section centroid (Fig. 4). With reference to the concentric tendon configuration, Fig. 2 provides an exploded view which summarizes the forces exchanged between the portions of the post-tensioned element before corrosion. The prestressing force acting in the cable is equal to P_1 throughout the entire length of the tendon (Assumption #7) and it is also completely and homogeneously transmitted to the concrete in all zones A, B and C, leading to a uniform compressive stress distribution equal to P_1/A_{cn}.

In the condition after corrosion, as previously stated in the problem formulation, from Assumption #8, the prestressing steel area is reduced from initial value A_{p1} to residual value A_{p2}, hence the prestressing steel area ratio is introduced as:

$$\rho = A_{p2}/A_{p1} < 1 \tag{1}$$

From the fundamental Assumption #10, the reduction of the prestressing steel area has two simultaneous effects, namely: (I) a loss of the prestressing force and (II) a stress redistribution of the residual prestressing steel area. Hence:

$$A_{p2} < A_{p1} \quad \text{and} \quad \begin{cases} P_2 < P_1 & \text{effect I} \\ \sigma_2 \neq \sigma_1 & \text{effect II} \end{cases} \tag{2}$$

where P_1 and P_2 are the prestressing forces (i.e. the forces exchanged between the two materials: prestressing steel and surrounding concrete) before and after corrosion, respectively, while σ_1 and σ_2 are the stresses in the cable before and after corrosion, respectively:

$$\sigma_1 = \frac{P_1}{A_{p1}} \quad \text{and} \quad \sigma_2 = \frac{P_2}{A_{p2}} \tag{3}$$

Regarding effect I, since P_1 is the prestressing force introduced at the act of steel tensioning and then evaluated after the immediate and time-dependent losses, it cannot increase unless the cables are re-tensioned. Hence, P_2, which is the prestressing force after corrosion acting on the steel and the concrete, is necessarily smaller than P_1.

Regarding effect II, three cases are possible: $\sigma_2 < \sigma_1$, $\sigma_2 = \sigma_1$, $\sigma_2 > \sigma_1$. It can be shown that the first two cases lead to a solution which

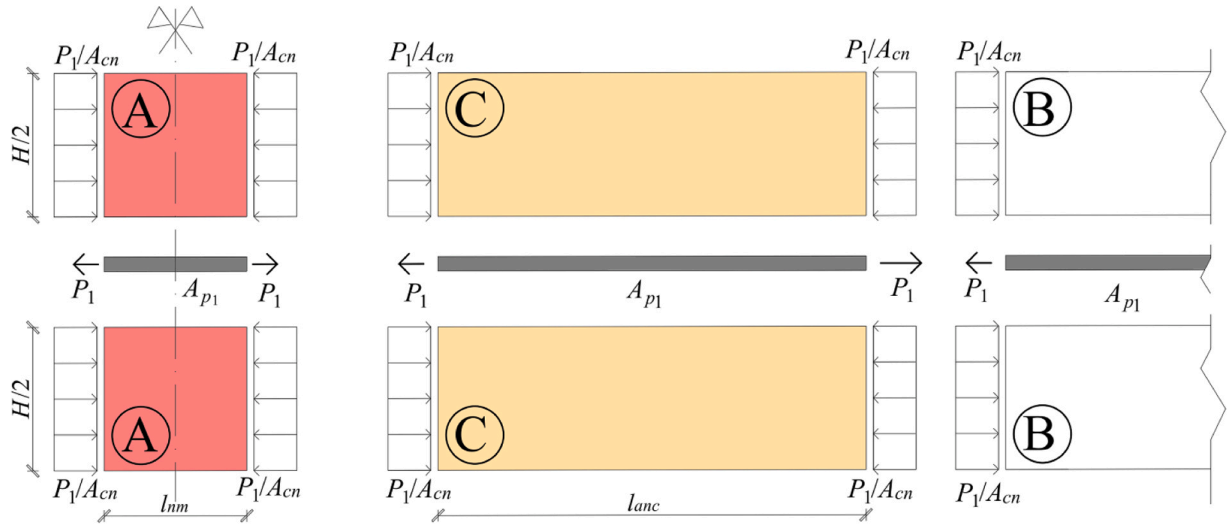

Fig. 2. Exploded view of the considered post-tensioned concrete element showing the coactive state before corrosion in the case of a concentric tendon.

is either only congruent or only balanced, and therefore not physically consistent. Consequently, in the following developments, the third case is considered and shown to be correct *a posteriori*.

From a mathematical point of view, the third case $\sigma_2 > \sigma_1$ occurs when $\frac{P_2}{P_1} > \frac{A_{p2}}{A_{p1}}$, i.e:

$$\rho < \rho_P \tag{4}$$

where $\rho = A_{p2}/A_{p1}$ is the prestressing steel area ratio and $\rho_P = P_2/P_1$ is here defined as the prestressing force ratio. From a physical point of view, it means that $\sigma_2 > \sigma_1$ occurs when the normalized reduction in the prestressing steel area is higher than the normalized reduction of the prestressing force, i.e. $1 - \rho > 1 - \rho_P$.

In the following, the analytical developments are carried out to quantitatively assess these effects by solving the hyperstatic problem of the residual coactive state, based on equilibrium and compatibility conditions, as schematically illustrated in Fig. 3.

Fig. 3 summarizes the forces exchanged between the cable and the transformed section A_{cn} (including concrete and ordinary steel only) after corrosion (equilibrium condition). In detail, inside the zone lacking mortar (zone A), since $\sigma_2 > \sigma_1$, the cable undergoes an elongation Δl_p. Due to the development of adherence in the adjacent zones (transition zones C and bonded zones B), the mean elongation Δl_p in the cable equals the elongation Δl_c (loss of shortening) in the concrete of zone A:

$$\Delta l_p = \Delta l_c \tag{5}$$

This is also consistent with the fact that the initial prestressing force P_1 is reduced to a residual prestressing force P_2 (effect I), and since $P_2 < P_1$, the reduction of the prestressing force in the concrete generates a decompression $\Delta P = P_1 - P_2$, which is consistent with the elongation in the concrete.

Due to Assumption #8 (in the entire zone A the cable is unbonded), the elongations in the cable and in the concrete may be rewritten in terms of mean strain variations, in the cable $\Delta\varepsilon_p$ and in the concrete $\Delta\varepsilon_c$, that occur along the entire length l_{nm}:

$$\Delta\varepsilon_p \cdot l_{nm} = \Delta\varepsilon_c \cdot l_{nm} \tag{6}$$

Therefore, the compatibility condition written in terms of elongations leads to the following equality of strain variations:

$$\Delta\varepsilon_p = \Delta\varepsilon_c \tag{7}$$

where: $\Delta\varepsilon_p = \varepsilon_{p,2} - \varepsilon_{p,1}$ and $\Delta\varepsilon_c = \varepsilon_{c,2} - \varepsilon_{c,1}$, leading to:

$$\varepsilon_{p,2} - \varepsilon_{p,1} = \varepsilon_{c,2} - \varepsilon_{c,1} \tag{8}$$

Fig. 4 shows the strain diagrams for cross-sections in the three

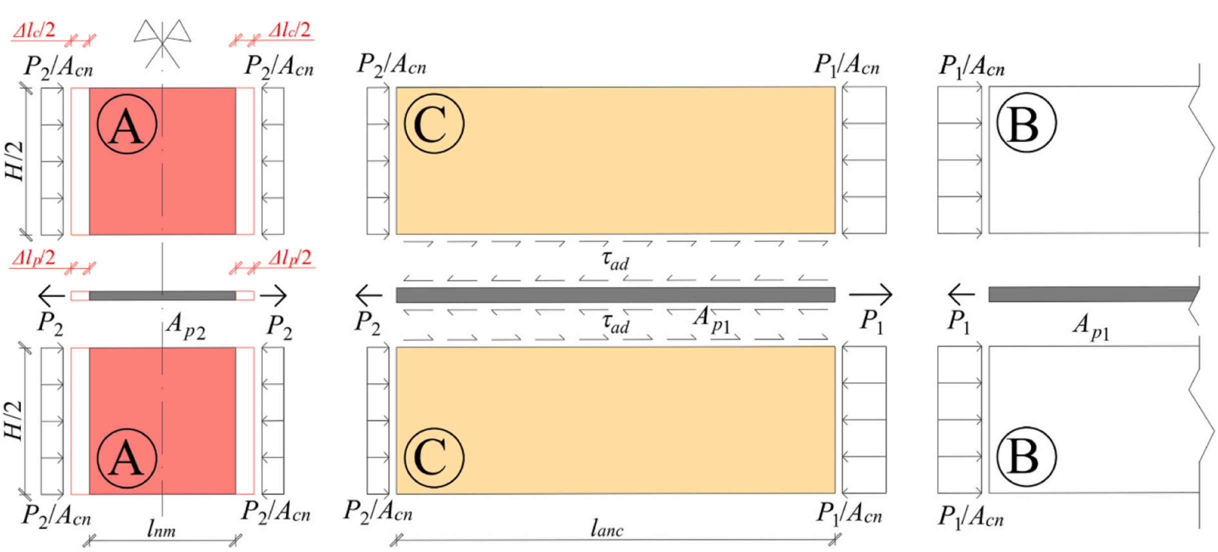

Fig. 3. Exploded view of the considered post-tensioned concrete element showing the coactive state after corrosion in the case of a concentric tendon.

considered zones. For each cross-section, the strain diagrams are referred to two reference systems which differ for the two materials to properly account for the prestressing coactive state [23,25,26]: (i) one for the concrete including the ordinary reinforcement, whose zero-strain reference line is indicated with ε_{Acn}, and (ii) another one for the prestressing steel only, whose zero-strain reference line is indicated with ε_{Ap}. For both reference systems, tension/elongation (+) is represented on the left side, while compression/shortening (-) is represented on the right side.

The strain diagram in the concrete is obviously uniform due to the concentric tendon configuration. A comparison is shown between condition 1, representing the strain diagram before corrosion, and condition 2, representing the strain diagram after corrosion. In detail, as formulated in 2, in zone A the two strain diagrams (e.g. either $\varepsilon_{c,1}$ and $\varepsilon_{p,1}$ for the condition before corrosion, or $\varepsilon_{c,2}$ and $\varepsilon_{p,2}$ for the condition after corrosion) are independent due to the fact that the cable is unbonded (i.e. the distance between the two zero-strain reference lines is arbitrary), while in zone B the two strain diagrams are connected due to the fact that the cable is bonded (i.e. the distance between the two zero-strain reference lines is fixed and equal to $\varepsilon_{c,1} + \varepsilon_{p,1}$). In the transition zone C, the strain diagrams are characterized by intermediate behavior which is not critical for the analytical developments presented in this research study. Going from the condition before corrosion to the condition after corrosion, in zone A the strain diagrams change (the concrete undergoes the decompression $\Delta\varepsilon_c$ and the prestressing steel undergoes the elongation $\Delta\varepsilon_p$), while in zone B the strain diagrams do not change. Due to Assumption #2, the concrete strain and the cable strain in zone A are given by:

$$(Condition\ 1 - before\ corrosion)\quad \begin{aligned} \epsilon_{c,1} &= -\frac{P_1}{E_c \cdot A_{cn}} \\ \epsilon_{p,1} &= +\frac{P_1}{E_p \cdot A_{p1}} \end{aligned} \tag{9}$$

$$(Condition\ 2 - after\ corrosion)\quad \begin{aligned} \epsilon_{c,2} &= -\frac{P_2}{E_c \cdot A_{cn}} \\ \epsilon_{p,2} &= +\frac{P_2}{E_p \cdot A_{p2}} \end{aligned} \tag{10}$$

where the "-" sign means shortening, while the "+ " sign means elongation. All the forces (P_1 and P_2) are always considered with their absolute values; and the signs are thus responsible for the identification of physical elongation or shortening. Consequently, Eq. (8) can be rewritten as follows:

$$\frac{P_2}{E_P A_{p2}} - \frac{P_1}{E_P A_{p1}} = \frac{P_1 - P_2}{E_c A_{cn}} \tag{11}$$

After a few mathematical steps, the residual prestressing force can be obtained from Eq. (11) as follows:

$$P_2 = \rho \frac{A_{cn} + n_p A_{p1}}{A_{cn} + n_p \rho A_{p1}} P_1 \tag{12}$$

or, equivalently, the prestressing force ratio is obtained as:

$$\rho_P = \frac{P_2}{P_1} = \rho \frac{A_{cn} + n_p A_{p1}}{A_{cn} + n_p \rho A_{p1}} \tag{13}$$

From Eq. (12), it is possible to observe that: if $\rho = 0$, then $P_2 = 0$, which corresponds to the total loss of the cable as a result of extensive corrosion; if $\rho = 1$, then $P_2 = P_1$, which corresponds to no corrosion and thus no loss of the prestressing force; if $0 < \rho < 1$, then $P_2 < P_1$, which corresponds to loss of the prestressing force.

Eq. (13) clearly highlights that the prestressing force is reduced by a different amount than the prestressing steel area and that, specifically, the loss of the prestressing force is smaller than the reduction in the prestressing steel area, since $\rho_P > \rho$, being $\rho \leq 1$.

The stress in the prestressing cable is then simply obtained as:

$$\sigma_2 = \frac{P_2}{A_{p2}} = \frac{\rho_P P_1}{\rho A_{p1}} = \frac{\rho_P}{\rho}\sigma_1 \tag{14}$$

which leads to:

$$\sigma_2 = \frac{A_{cn} + n_p A_{p1}}{A_{cn} + n_p \rho A_{p1}} \sigma_1 \tag{15}$$

or, equivalently, the cable stress ratio ρ_σ can be introduced as:

$$\rho_\sigma = \frac{\sigma_2}{\sigma_1} = \frac{A_{cn} + n_p A_{p1}}{A_{cn} + n_p \rho A_{p1}} \tag{16}$$

From Eq. (15), it is possible to observe that: if $\rho = 0$, then σ_2 loses its significance, since there is no residual area in the cable; if $\rho = 1$, then $\sigma_2 = \sigma_1$, which corresponds to no increase in the stress of the prestressing steel area, since no corrosion occurs; if $0 < \rho < 1$, then $\sigma_2 > \sigma_1$, which confirms that the stress increases after corrosion.

Eq. (16) clearly indicates that the stress in the residual prestressing steel area increases after corrosion, since the term $A_{cn} + n_p A_{p1}$ is larger than $A_{cn} + n_p \rho A_{p1}$. This result finally confirms that the third case $\sigma_2 > \sigma_1$ (regarding the stress redistribution in the cable) proves to be correct and physically consistent, since both equilibrium and compatibility are

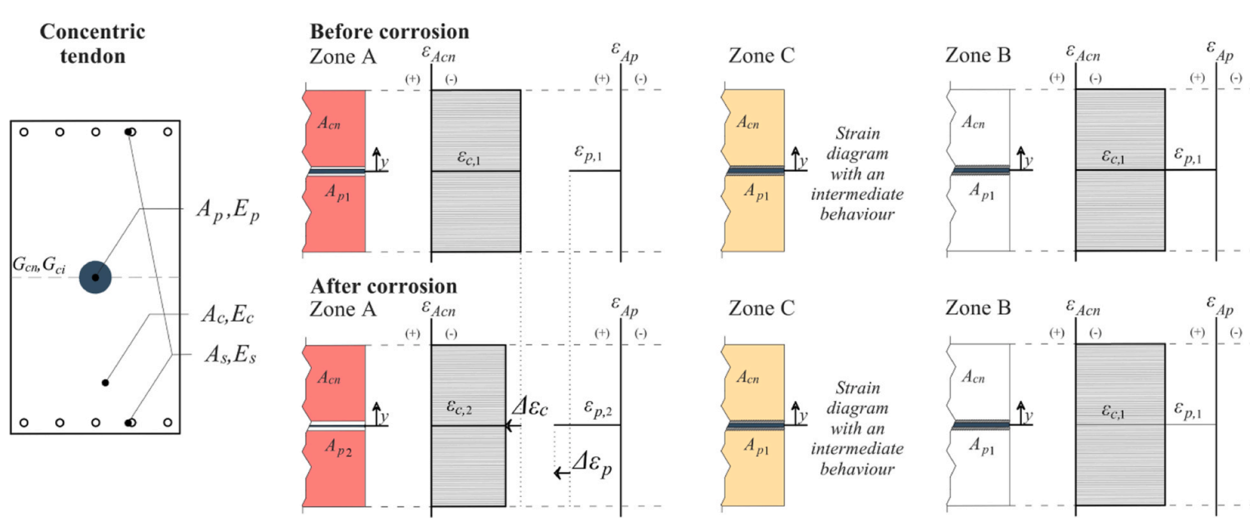

Fig. 4. Strain diagrams for the concentric tendon before and after corrosion.

satisfied. It is worth noticing that the following relationships hold between the three introduced ratios:

$$\rho_P = \rho \cdot \rho_\sigma \tag{17}$$

$$\rho_\sigma = \frac{\rho_P}{\rho} \tag{18}$$

From Eqs. (17) and (18) the prestressing steel area ratio $\rho = A_{p2}/A_{p1}$ (which is always smaller than 1, if corrosion occurs) clearly leads to two effects on the considered tendon. In particular, these effects can be considered complementary and are quantitatively described by the reduction of prestressing force and the increase in cable stress. Eq. (17) highlights the direct proportionality between ρ_P and ρ, while Eq. (18) highlights the inverse proportionality between ρ_σ and ρ.

The validity of the initial assumption concerning the third case $\sigma_2 > \sigma_1$ for stress redistribution in the cable is further supported by the following observations on the other two cases.

Considering the case $\sigma_2 = \sigma_1$, i.e. assuming that the stress in the prestressing cable remains constant, implies that the cable does not undergo any elongation. This, however, would be incompatible with the elongation of the concrete caused by the reduction in prestressing force $(P_2 < P_1)$.

Considering the case $\sigma_2 < \sigma_1$, the cable is expected to shorten, thereby decreasing its initial elongation. As a result, the concrete in zone A must also experience additional shortening. This, however, would be incompatible with the reduction in prestressing force $(P_2 < P_1)$.

The elongation $\Delta l = \Delta l_p = \Delta l_c$ due to the prestress loss inside the length l_{nm} (in zone A) is calculated as:

$$\Delta l = \frac{P_1 - P_2}{E_c A_{cn}} \cdot l_{nm} \tag{19}$$

In zone B, due to the adherence restored beyond the interface between zones A and C and the equilibrium provided by the shear stresses τ_{ad} that develop in the transition zone C, the coactive state in the after-corrosion condition is identical to the coactive state in the before-corrosion condition. In detail, inside the transition zone C, shear stresses τ_{ad} arise to restore the equilibrium perturbed by the prestressing force variation ΔP, according to the following formula:

$$\Delta P = P_1 - P_2 = \tau_{ad} \cdot l_{anc} \cdot s_b \tag{20}$$

where s_b is an equivalent length describing the contact surface perimeter between the prestressing steel A_{p1} and the surrounding mortar, which could vary according to the prestressing steel geometry and arrangement.

In order to quantify the results of the proposed analytical formulation in terms of prestressing force reduction and cable stress increase, sensitivity analyses are conducted on the main parameters affecting the analytical model. As previously commented, the effect of corrosion is mainly governed by the prestressing steel area ratio ρ, which can vary between 0 and 1, $\rho = 0$ representing a limit condition of complete corrosion (failure) of the cable, and $\rho = 1$ describing the other limit condition of no corrosion at all. However, in the presented analytical model, according to the behavior of post-tensioned concrete elements with mortar injection, the variation of the coactive state in the prestressing steel reinforcement is not only dependent on the amount of residual prestressing steel area but also on the collaborating concrete section. In fact, it is worth noting that the concentric tendon formulation described by Eq. (13) in terms of prestressing forces and Eq. (16) in terms of cable stresses, can be reformulated as follows:

$$\rho_P = \frac{P_2}{P_1} = \rho \frac{(1 + n_p \cdot \rho_R)}{(1 + n_p \cdot \rho \cdot \rho_R)} \tag{21}$$

$$\rho_\sigma = \frac{\sigma_2}{\sigma_1} = \frac{(1 + n_p \cdot \rho_R)}{(1 + n_p \cdot \rho \cdot \rho_R)} \tag{22}$$

where the reinforcement ratio ρ_R is introduced, defined as the ratio between the amount of initial prestressing steel area and the transformed section area, which includes concrete and ordinary reinforcement only:

$$\rho_R = \frac{A_{p1}}{A_{cn}} \tag{23}$$

In order to visualize the results provided by the analytical model, the two ratios ρ and ρ_R governing the prestressing coactive state variation are evaluated in the following ranges: ρ= 0–1 and ρ_R = 0.1%–10%. The selected range of ρ_R was chosen to cover lower and upper bounds representative of most practical cases involving internal post-tensioned tendons. In particular, values around ρ_R = 0.1% correspond to structural elements characterized by a limited amount of prestressing reinforcement with respect to the net concrete cross-section (i.e. bridge girders), whereas values approaching ρ_R = 10% are representative of elements characterized by a high proportion of prestressing reinforcement relative to the resisting cross-section (i.e. prestressed stays). Fig. 5 displays the obtained results in terms of prestressing force reduction (Fig. 5a) and cable stress increase (Fig. 5b) as a function of the prestressing steel area ratio ρ, for increasing values of ρ_R.

The following observations can be made:

- For small reinforcement ratios ρ_R, the prestressing force ratio ρ_P is linear with and roughly equal to the prestressing steel area ratio ρ. For high reinforcement ratios ρ_R, ρ_P shows a non-linear dependence on ρ, showing a slightly smaller reduction of the prestressing force (with respect to the area reduction). For instance, for $\rho = 0.4$ corresponding to a 60% steel area reduction, $\rho_P \cong 0.4$ corresponding to a 60% prestressing force reduction for small reinforcement ratios (e.g. close to $\rho_R \cong 0.1\%$), while $\rho_P \cong 0.5$ corresponding to a 50% prestressing force reduction for high reinforcement ratios (e.g. close to $\rho_R \cong 10\%$).
- For small reinforcement ratios ρ_R, the cable stress ratio ρ_σ is almost constant and roughly equal to 1. For high reinforcement ratios ρ_R, ρ_σ shows a non-linear dependence on ρ, assuming values far larger than 1. For instance, for $\rho = 0.4$, $\rho_\sigma \cong 1$ for small reinforcement ratios (e.g. close to $\rho_R \cong 0.1\%$), while $\rho_\sigma \cong 1.3$ for high reinforcement ratios (e.g. close to $\rho_R \cong 10\%$). In other words, in the former case there is no substantial increase of the stress in the residual steel area, while in the latter case the increase of the cable stress is around 30%.

It is worth emphasizing that the stress amplification predicted by the analytical formulation (Fig. 5b) must be interpreted within the validity domain of the adopted mechanical assumptions, and specifically under the hypothesis of linear elastic material behavior of the prestressing steel (Assumption #2). If this condition is violated (once the cable is yielded), the active effect of prestressing is lost and sudden brittle rupture may occur. In mathematical terms, to ensure consistency with the elastic domain of the prestressing steel, the following condition must be satisfied:

$$\sigma_2 < f_{py} \tag{24}$$

or, equivalently, in normalized terms:

$$\rho_\sigma < \frac{f_{py}}{\sigma_1} \tag{25}$$

where f_{py} is the assumed yielding strength. Combining Eq. (25) with Eq. (22), the following applicability condition in terms of prestressing steel area ratio is obtained:

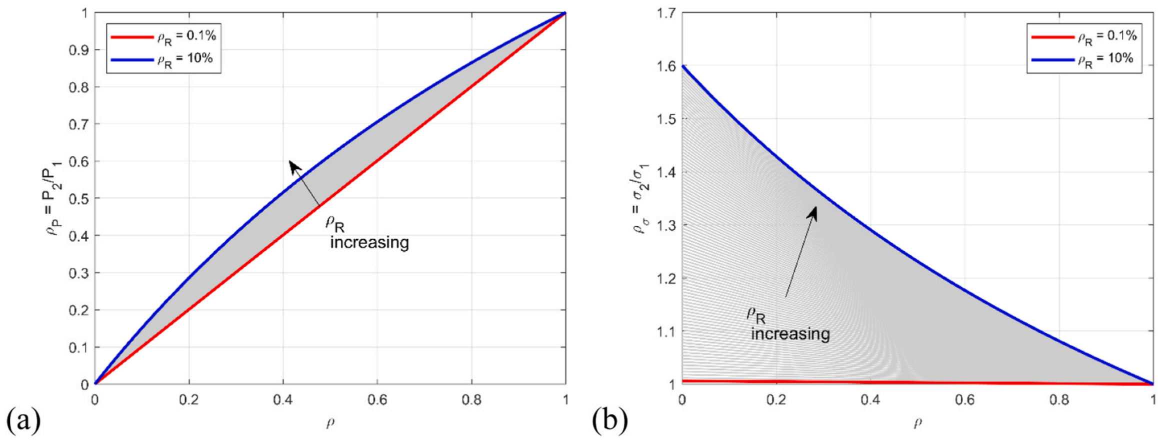

Fig. 5. Sensitivity analyses conducted for different values of prestressing steel area ratio and increasing values of reinforcement ratio on: (a) prestressing force ratio ρ_P; (b) cable stress ratio ρ_σ.

$$\rho > \rho_{crit} = \frac{1 + n_p \cdot \rho_R - \left(\frac{f_{py}}{\sigma_1}\right)}{n_p \cdot \rho_R \cdot \left(\frac{f_{py}}{\sigma_1}\right)} \tag{26}$$

The condition $\rho > \rho_{crit}$ defines the applicability range of the analytical formulation, where ρ_{crit} is a critical value of the prestressing steel area ratio, below which the stress predicted by the model exceeds the yield strength, and the prestressing force is no longer active. It should be noted that, depending on the input parameters (n_p, ρ_R, f_{py}, σ_1), ρ_{crit} may also take negative values. However, if $\rho_{crit} \le 0$, then Eq. (26) is trivially satisfied since $\rho > 0$ by definition and, consequently, σ_2 is always smaller than f_{py}. In other words, the stress increase due to corrosion does not lead to yielding of prestressing steel. As illustrative examples, assuming $n_p = 6$, $\sigma_1 = 1200$ MPa and $f_{py} = 1600$ MPa, for the case of ρ_R= 0.1%, the results plotted with the red line in Fig. 5b are always valid since $\rho_{crit} < 0$, whilst, for the case of ρ_R= 10%, the results plotted with the blue line in Fig. 5b are valid only when $\rho > \rho_{crit} = 0.33$.

3.2. Eccentric tendon

In order to extend the formulation of a post-tensioned element with concentric tendon to a more generalized post-tensioned element with eccentric tendon, the same approach has been applied considering a post-tensioned beam having the equivalent cable with a given eccentricity $e_{cn} \neq 0$, with respect to the center of mass of the transformed cross-section that includes concrete and ordinary reinforcement only (Fig. 6). In this case, the deformation inside the concrete is affected also by the bending moment contribution induced by the cable eccentricity.

Fig. 6 shows the strain diagrams before and after corrosion for zones A, B and C. Similarly to the concentric tendon configuration, the strain distribution varies depending on whether the cable segment is bonded or unbonded. Unlike the concentric tendon configuration, due to the bending moment contribution induced by the cable eccentricity and due to Assumption #1, the strain diagrams (before and after corrosion) in the concrete are linear. Analogously to Fig. 4, Fig. 6 shows that going from the condition before corrosion to the condition after corrosion, in zone A the strain diagrams change, while in zone B the strain diagrams do not change. Specifically, in zone A the concrete undergoes the decompression $\Delta\varepsilon_{Gcn}$ at the center of mass fiber and the decompression $\Delta\varepsilon_{cp}$ at the concrete fiber corresponding to the prestressing steel position, thus leading to a variation also in the curvature of the cross-section.

In zone A, in general, the strain diagram in the concrete for condition before corrosion (subscript 1) is described by the following formula:

$$\varepsilon_{c,1}(y) = -\frac{P_1}{E_c \cdot A_{cn}} - \frac{P_1 \cdot (-e_{cn})}{E_c \cdot J_{cn}} \cdot y \tag{27}$$

where e_{cn} is the absolute value of the eccentricity, and y represents the distance of a generic cross-section fiber from the neutral axis, as computed with reference to the cross-section that includes concrete and ordinary reinforcement only (positive value upwards).

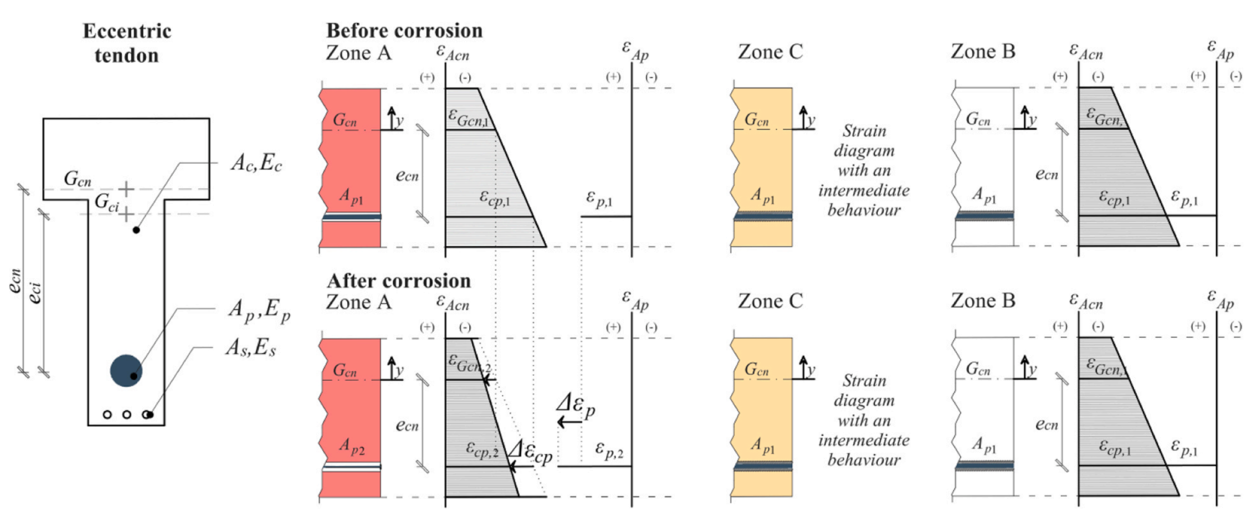

Fig. 6. Strain diagrams for the eccentric tendon before and after corrosion.

In zone A, specifically, the strain at the center of mass ε_{Gcn}, the strain at the concrete fiber corresponding to the tendon position ε_{cp}, and the strain in the tendon ε_p are provided hereafter, for condition before corrosion (pedex 1) and for condition after corrosion (subscript 2):

$$(Condition\ 1 - before\ corrosion)\quad \varepsilon_{Gcn,1} = -\frac{P_1}{E_c \cdot A_{cn}}$$
$$\varepsilon_{cp,1} = -\frac{P_1}{E_c \cdot A_{cn}} - \frac{P_1}{E_c \cdot J_{cn}} e_{cn}{}^2 \tag{28}$$
$$\varepsilon_{p,1} = +\frac{P_1}{E_p \cdot A_{p1}}$$

$$(Condition\ 2 - after\ corrosion)\quad \varepsilon_{Gcn,2} = -\frac{P_2}{E_c \cdot A_{cn}}$$
$$\varepsilon_{cp,2} = -\frac{P_2}{E_c \cdot A_{cn}} - \frac{P_2}{E_c \cdot J_{cn}} e_{cn}{}^2 \tag{29}$$
$$\varepsilon_{p,2} = +\frac{P_2}{E_p \cdot A_{p2}}$$

From condition 1 to condition 2, given the fundamental Assumption #10, the prestressing force decreases ($P_2 < P_1$) and the cable stress increases ($\sigma_2 > \sigma_1$).

This leads to a reduction of the compressive strains all over the concrete, with a higher reduction in the portion where the equivalent cable is located. With specific reference to the concrete fiber corresponding to the cable position, this reduction equals:

$$\Delta\varepsilon_{cp} = \varepsilon_{cp,2} - \varepsilon_{cp,1} \tag{30}$$

In parallel, the strain level in the cable increases by the following quantity:

$$\Delta\varepsilon_p = \varepsilon_{p,2} - \varepsilon_{p,1} \tag{31}$$

In zone B, corrosion occurring in zone A does not have any effects (in terms of strains) due to the persistence of the adherence in zone B and due to the anchorage provided by transition zone C (assumption #9), for the variation of the prestressing force, indicated as "secondary anchorage effect" in [27].

The same approach adopted for the concentric tendon configuration is followed, starting from the compatibility equation:

$$\Delta\varepsilon_{cp} = \Delta\varepsilon_p \tag{32}$$

Introducing Eqs. (30) and (31) in Eq. (32) leads to the analytical formula providing the residual prestressing force:

$$P_2 = \rho \cdot \frac{A_{cn}J_{cn} + n_p A_{p1} J_{cn} + n_p A_{p1} A_{cn} e_{cn}^2}{A_{cn}J_{cn} + n_p \rho A_{p1} J_{cn} + n_p \rho A_{p1} A_{cn} e_{cn}^2} \cdot P_1 \tag{33}$$

and – through Eqs. (1) and (3) – to the analytical formula providing the stress inside the cable after corrosion:

$$\sigma_2 = \frac{A_{cn}J_{cn} + n_p A_{p1} J_{cn} + n_p A_{p1} A_{cn} e_{cn}^2}{A_{cn}J_{cn} + n_p \rho A_{p1} J_{cn} + n_p \rho A_{p1} A_{cn} e_{cn}^2} \cdot \sigma_1 \tag{34}$$

Eqs. (33) and (34) are the fundamental results of this research study. They clearly represent the generalization of Eqs. (12) and (15). Actually, by imposing $e_{cn} = 0$ in Eqs. (33) and (34), Eqs. (12) and (15) are obtained. Moreover, with respect to the concentric tendon configuration, in the eccentric tendon configuration, the presence of an eccentricity slightly modifies the prestressing force ratio and the cable stress ratio. Indeed, the analytical formulations of the here proposed modification factors to account for corrosion-induced variation of the prestressing coactive state (i.e. the prestressing force ratio ρ_P and the cable stress ratio ρ_σ) are given by:

$$\rho_P = \frac{P_2}{P_1} = \rho \cdot \frac{1 + n_p \cdot \rho_R + n_p \cdot \rho_R \cdot \rho_J}{1 + n_p \cdot \rho \cdot \rho_R + n_p \cdot \rho \cdot \rho_R \cdot \rho_J} \tag{35}$$

$$\rho_\sigma = \frac{\sigma_2}{\sigma_1} = \frac{1 + n_p \cdot \rho_R + n_p \cdot \rho_R \cdot \rho_J}{1 + n_p \cdot \rho \cdot \rho_R + n_p \cdot \rho \cdot \rho_R \cdot \rho_J} \tag{36}$$

where $\rho_J = \left(A_{cn} \cdot e_{cn}{}^2\right)/J_{cn}$ is a new parameter accounting for the eccentricity of the equivalent cable. Specifically, it represents the ratio of the moment of inertia provided by the area A_{cn}, as calculated with respect to an axis passing through the prestressing steel area, to the moment of inertia of the cross-section including only concrete and ordinary steel J_{cn}. Note that, of course, for a concentric tendon, $\rho_J = 0$. Typically, ρ_J assumes positive values, which can be far larger than one.

Analogously to the concentric case, by imposing the condition $\sigma_2 < f_{py}$ (Eq. (24)), the applicability condition $\rho > \rho_{crit}$ of the analytical formulation is obtained, where, in this case, the critical value ρ_{crit} is generalised as a function of both the reinforcement ratio ρ_R and the moment of inertia ratio ρ_J:

$$\rho_{crit} = \frac{1 + n_p \cdot \rho_R \cdot (1 + \rho_J) - \left(\frac{f_{py}}{\sigma_1}\right)}{n_p \cdot \rho_R \cdot (1 + \rho_J) \cdot \left(\frac{f_{py}}{\sigma_1}\right)} \tag{37}$$

Fig. 7a and b show a 3D representation of the influence of ρ, ρ_R and ρ_J on the prestressing force ratio ρ_P and on the cable stress ratio ρ_σ. Specifically, the 3D representation shows ρ_P and ρ_σ as a function of ρ (varying from 0 to 1) and ρ_J (varying from 0 to 5), for two selected values of ρ_R (namely, 0.1% and 10%). On one hand, ρ_P has a linear and a slightly curvilinear variation with ρ, for small (red) and large (blue) values of ρ_R, respectively, while it is substantially not influenced by ρ_J. On the other hand, ρ_σ is approximately equal to 1 for all values of ρ and ρ_J for small (red) values of ρ_R, while it is noticeably affected by ρ_J only for small values of ρ for high (blue) values of ρ_R. From an engineering point of view, it is confirmed that, for small reinforcement ratios (red), the prestressing force ratio ρ_P is linear with and roughly equal to the prestressing steel area ratio ρ, and the cable stress ratio ρ_σ is almost constant and roughly equal to 1; these fundamental results are not affected by ρ_J. Instead, for high reinforcement ratios (blue), ρ_J considerably affects ρ_σ, but not ρ_P.

Fig. 8 provides two-dimensional plots to allow for a better quantification of the effects of the considered ratios. Fig. 8a shows the trends of the prestressing force ratio ρ_P as a function of the prestressing steel area ratio ρ, for the two values of $\rho_R = 0.1\%$ representing small values of reinforcement ratio, and $\rho_R = 10\%$ representing high values of reinforcement ratio, illustrating in more detail the effects of ρ_J. For instance, in the case of small values of ρ_R, $\rho = 0.4$ leads to $\rho_P \cong 0.4$ for all values of ρ_J. In the case of high values of ρ_R, $\rho = 0.4$ leads to $\rho_P \cong 0.52$ for $\rho_J = 0$ (e.g. concentric tendon) and to $\rho_P \cong 0.75$ for $\rho_J = 5$ (e.g. eccentric tendon). The analytical model indicates that, under identical geometric and corrosion conditions, the reduction of the prestressing force due to corrosion is generally smaller in the eccentric tendon compared to the corresponding concentric tendon. Indeed, the residual prestressing force P_2 is larger in the case of eccentric tendon. This indicates that, from the perspective of the residual prestressing force, the beam benefits from the eccentricity of the tendon, whereas the worst-case scenario for prestressing force reduction corresponds to the concentric tendon configuration. In parallel, Fig. 8b shows the trends of the cable stress ratio ρ_σ as a function of the prestressing steel area ratio ρ, for the two values of $\rho_R = 0.1\%$ and $\rho_R = 10\%$, illustrating in more detail the effects of ρ_J. For instance, in the case of small values of ρ_R, $\rho = 0.4$ leads to $\rho_\sigma \cong 1.004$ and $\rho_\sigma \cong 1.020$, for $\rho_J = 0$ and $\rho_J = 5$, respectively. In the case of high values of ρ_R, $\rho = 0.4$ leads to $\rho_\sigma \cong 1.290$ and $\rho_\sigma \cong 1.885$, for $\rho_J = 0$ and $\rho_J = 5$, respectively; the eccentric tendon displaying a higher increase of the prestressing stress in the cable due to corrosion with respect to the concentric one. This means that, from the perspective of the cable stress, the beam does not take advantage of the eccentricity of the tendon. The worst case for the cable stress increase due to corrosion is the eccentric tendon case.

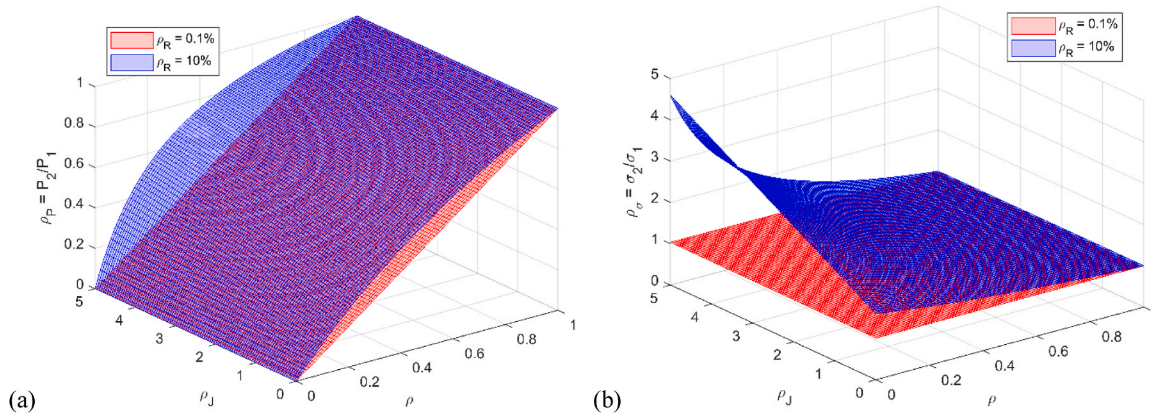

Fig. 7. 3D representation of the results of the analytical model for the eccentric tendon configuration as a function of ρ_J and ρ, for two selected values of ρ_R: (a) prestressing force ratio ρ_P; (b) cable stress ratio ρ_σ.

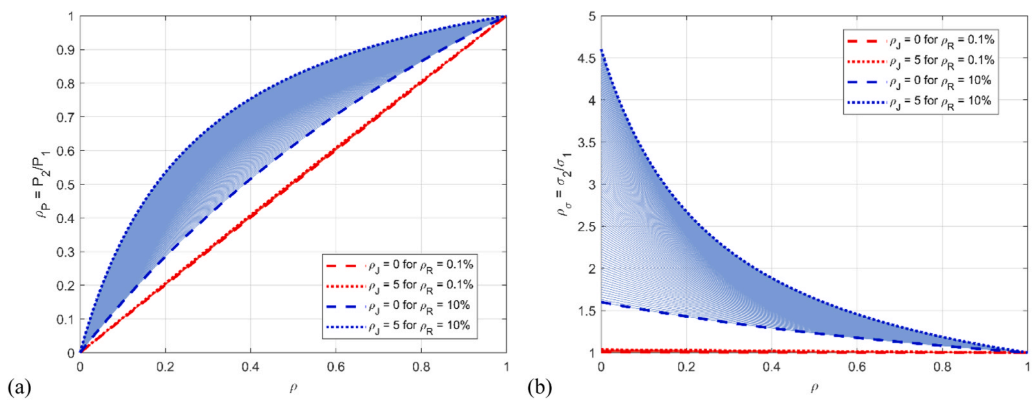

Fig. 8. 2D representation of the results of the analytical model for the eccentric tendon configuration as a function of ρ and ρ_J for small reinforcement ratio, ρ_R= 0.1%, and high reinforcement ratio, ρ_R= 10%: (a) prestressing force ratio ρ_P; (b) cable stress ratio ρ_σ.

4. Experimental validation

Setting up a test on a post-tensioned beam with internal tendons that simultaneously monitors both the initial uncorroded state and the subsequent (even artificially induced) corroded condition in the zone lacking mortar injection - using reliable sensors to measure prestressing force and cable stress - is difficult to implement and execute, thus still representing a highly challenging and relevant research topic for the engineering scientific community. As a result, experimental data are unavailable in the literature for post-tensioned elements with internal tendons, although some studies exist for elements with external tendons [9,28,29].

In this section, the results provided by the presented analytical model are compared with experimental data available for external grouted post-tensioned tendons. It should be noted, however, that the comparison requires caution due to the different range of reinforcement ratios involved (ρ_R = 30%–70%, instead of 0.1%–10%, which typically characterizes the cross-section with internal tendons), due to the fact that, in this case, the concrete area is assimilated to the grout area within the duct. Specifically, reference is made here to the work by Wood, Mckinstry and Lee [29]. The study experimentally investigates the structural effects of localized corrosion on four large-scale specimens of externally post-tensioned tendons. A summary of specimen characteristics and key parameters is provided in Table 1. In the specimen notation, the letter C or S indicates concrete or steel anchor block, respectively; while the number 40 or 70 represents the level of initial prestress (before corrosion), corresponding to 40% and 70% of the Guaranteed Ultimate Tensile Strength (GUTS). Each tendon specimen consisted of seven prestressing steel 0.6''-strands, composed of seven wires each (for a total number of 49 wires). The samples were enclosed in a plastic duct filled with grout. Damage was induced in a 30 cm-length segment, where duct and grout were deliberately removed, using a

Table 1
Specimen characteristics and key parameters from Wood, Mckinstry, and Lee [29].

Specimen	Initial Prestressing Force (kN)	% GUTS	Number of Strands	Strand Diameter (mm)	Corrosion Conditions	Number of Strands Corroded	Measured Parameters
C-40	778	42.6	7	15.2	Galvanic, gradual wire breakage	4	Residual tensile force, strains
C-70	1224	67.1	7	15.2	Galvanic, gradual wire breakage	5	Residual tensile force, strains
S-40	775	42.4	7	15.2	Galvanic, gradual wire breakage	5	Residual tensile force, strains
S-70	1241	68.0	7	15.2	Galvanic, gradual wire breakage	5	Residual tensile force, strains

galvanic corrosion cell in a controlled manner to progressively break individual wires. The residual tensile force was measured using a load cell and strains were measured using 6- mm foil gauges attached to two outer wires of each strand. Most of these gauges progressively debonded from the surface as the number of wire breaks increased, highlighting that it is challenging to obtain reliable strain measures for high prestress and corrosion levels. Further details on the specimens and test set-up are found in the original paper [29].

To enable a direct comparison between the presented analytical model and the experimental results, a correlation was established between the measured and analytical parameters describing the corrosion-induced damage, the residual tensile force and the stress in the strands.

In the experimental study, the corrosion-induced damage of each specimen was quantified by the number of wire breaks. In the presented analytical model, the damage index D represents the reduction in the cross-sectional area of the prestressing steel due to corrosion and is defined as $D = 1 - \rho$, where ρ denotes the ratio of the remaining (post-corrosion) area A_{p2} to the initial (pre-corrosion) area A_{p1} of the prestressing steel. The correlation between the experimentally observed number of wire breaks and the model's damage parameter is given by $D = 1 - \rho = 1 - A_{p2}/A_{p1} = (A_{p1} - A_{p2})/A_{p1} = N_b/N$, where N_b is the number of wire breaks and N is the total number of wires.

The experimental Normalized Residual Tensile Force, obtained as the ratio between the measured tensile force and the initial prestress level, directly correlates with the analytical definition of the prestressing force ratio ρ_P provided for the zone subjected to corrosion. Similarly, the stress measured experimentally in the corroded portion of the strands, expressed as a percentage of the Guaranteed Ultimate Tensile Strength (GUTS) of the prestressing steel, corresponds to the predicted stress in the tendon after corrosion denoted as σ_2. A correspondence with the cable stress ratio ρ_σ is obtained by normalizing the experimental post-corrosion stress by the initial prestress level for each specimen.

Fig. 9 shows the comparison between the predicted analytical parameters and the values measured experimentally as a function of the damage index D. This figure represents an adaptation - aligned with the nomenclature adopted in the present study - of Fig. 11 from the research work by Wood, McKinstry and Lee [29].

Overall, although it should be reiterated that the reinforcement ratio considered in this comparison is relatively high, the analytical results show good agreement with the experimental data, as the observed trends are well captured both qualitatively and quantitatively. Specifically, Fig. 9a shows that the experimentally measured prestressing force ratios lie between the predictions of the proposed analytical model and those of the simplified linear damage model adopted as a reference by Wood, McKinstry, and Lee [29], with the analytical model providing an upper bound to the experimental values. Similarly, Fig. 9b indicates that the analytical prediction of the cable stress ratio also represents an upper bound for the experimental measurements. For large damage indices (i.e., very small values of ρ), the analytical curve of the cable stress ratio exhibits a divergent exponential trend. This behavior is physically consistent, as the prestressing steel area ratio decreases faster than the prestressing force ratio (Eq. (4)), in accordance with equilibrium and compatibility requirements. Experimental data are available only up to intermediate damage levels and are affected by increasing measurement uncertainty. Within the investigated range, the proposed formulation provides a conservative estimate of the cable stress.

5. Numerical application to existing bridge elements

In this section, the ready-to-use formulas developed in 3.2 are applied to real case-study bridges to contextualize their practical applications and to identify the typical range of numerical values assumed by the prestressing force ratio ρ_P and by the cable stress ratio ρ_σ in possible corrosion scenarios.

Three case-studies are considered in this research work, each one referable to a specific post-tensioned element: (1) a prestressed concrete stay in a cable-stayed bridge, (2) a multi-cell caisson-box deck of a simply-supported bridge, (3) a multiple-spine box girder in a continuous bridge. Fig. 10 shows the overview and the considered cross-sections for each illustrative example.

The first illustrative example refers to the prestressed concrete stays that characterized the Polcevera Viaduct (Genova, Italy) designed by Riccardo Morandi and collapsed in 2018 [30,31]. The second illustrative example refers to a prestressed concrete railway bridge designed by Mario Paolo Petrangeli, and inaugurated in 1976 [32,33], located in Napoli (Italy). The third illustrative example refers to the Stronetta viaduct [34], built by the Autostrade S.p.A. Italian company during the construction of the so-called Autostrada dei Trafori (A26) highway extension. For the purposes of this study, the data regarding the cross-section geometry and the prestressing reinforcement of the three case-studies have been deduced from the literature or original documentation and are reported in Table 2.

A quantification of the initial coactive state before corrosion has been performed for the case-studies. The value of the prestressing force P_1 has been computed according to Eurocode 2 [35] and Italian Technical Code [36]. In case the initial value of stress just after tensioning σ_0 at the active end was not available from the original drawings (e.g. examples 1 and 3), it has been evaluated according to Eurocode 2 as $\sigma_0 = \min\left(0.75 f_{pk} \ ; \ 0.85 f_{p0.1k} \right)$, where f_{pk} is the characteristic tensile strength of the prestressing steel and $f_{p0.1k}$ is the characteristic 0.1% proof-stress of the prestressing steel. Then, σ_1 has been evaluated considering 15% of prestress losses due to rheological effects. This value is assumed as representative of typical total long-term prestress losses associated with creep, shrinkage of concrete, and relaxation of prestressing steel, in accordance with commonly adopted ranges as

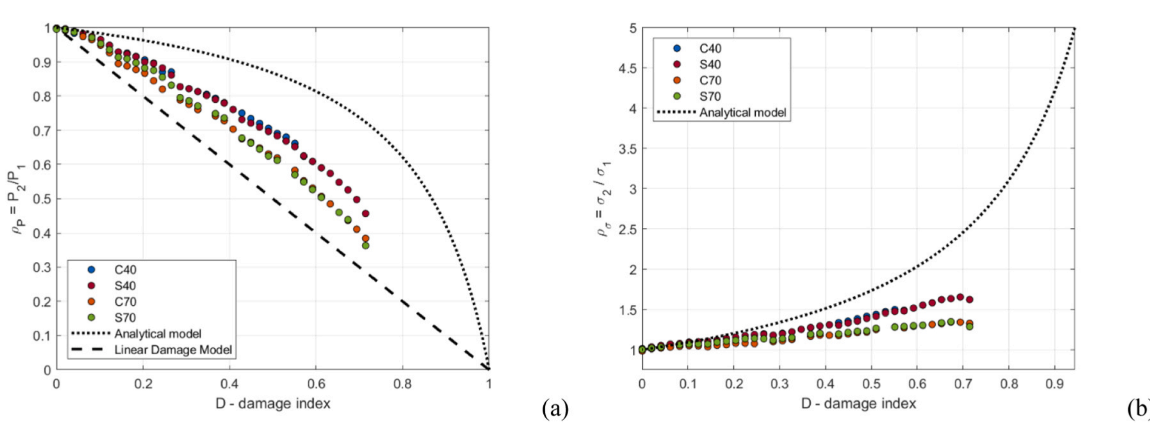

Fig. 9. Validation of the proposed analytical formulations for (a) the prestressing force ratio ρ_P and (b) the cable stress ratio ρ_σ.

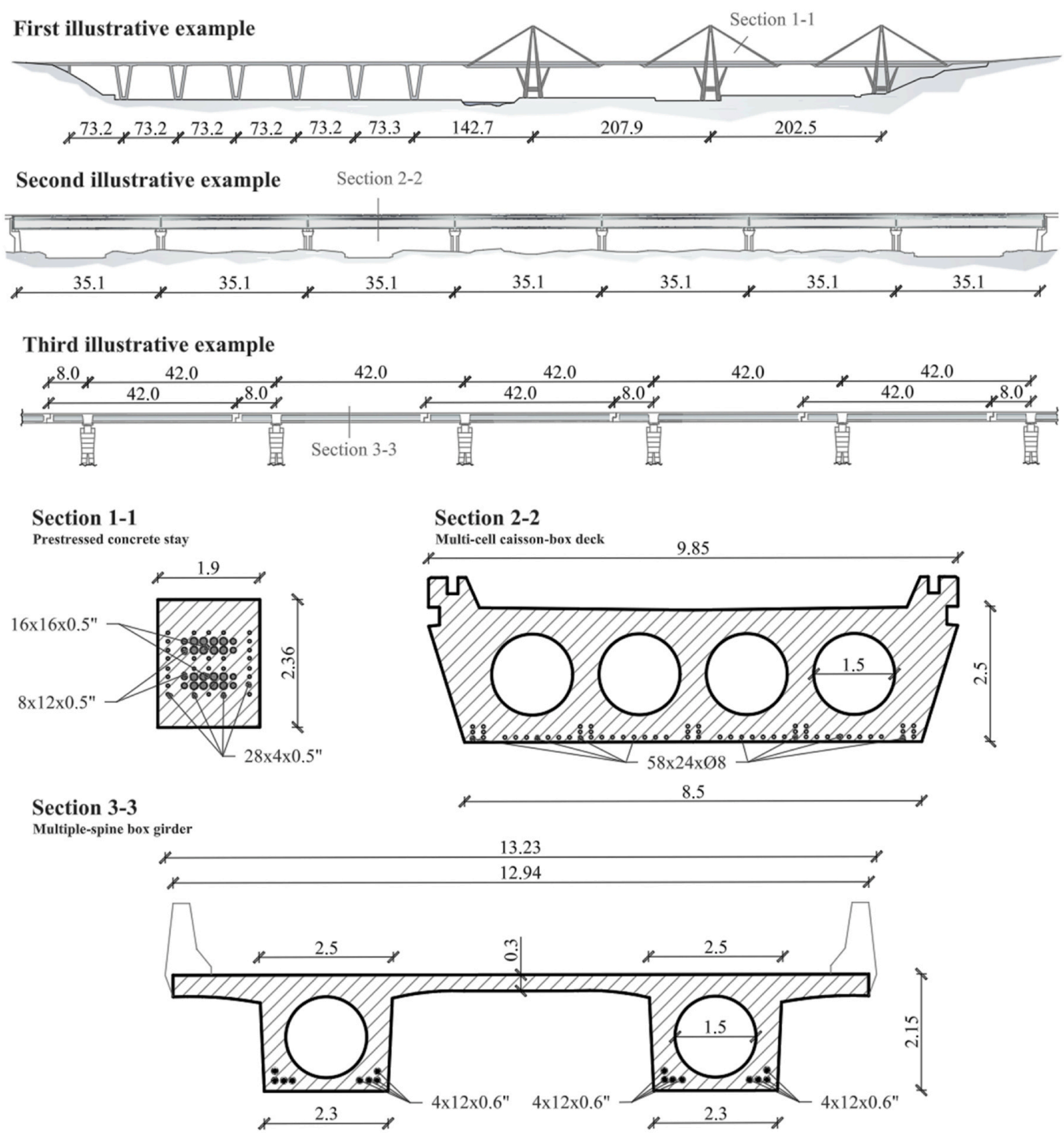

Fig. 10. Overview and considered cross-sections for the three illustrative examples. All dimensions are in meters (m), unless otherwise specified.

Table 2
Parameters of the considered case-studies.

Data	Units	Example 1 Prestressed concrete stay	Example 2 Multi-cell caisson-box deck	Example 3 Multiple-spine box girder
A_{cn}	m^2	1.05	16.45	9.68
A_p	mm^2	43152	69970	26688
n_s, n_p	-	6	6	6
J_{cn}	m^4	0.10	12.10	4.60
$e_{cn,\max}$	m	0	1.22	1.33
ρ_R	-	4.09%	0.43%	0.28%
ρ_J	-	0	2.02	3.72
σ_1	MPa	1200	1100	1200
P_1	kN	51782	76967	32026

computed from codes and regulations [35,37,38]. The stresses σ_1 and the corresponding forces P_1 are reported in Table 2. For all three examples, ρ_{crit} is smaller than zero, so that the analytical formulation is valid over the entire range (0,1) of ρ.

Fig. 11 describes the trends of the prestressing force ratio $\rho_P = P_2/P_1$ (Fig. 11a) and of the cable stress ratio $\rho_\sigma = \sigma_2/\sigma_1$ (Fig. 11b) for different values of prestressing steel area ratio $\rho = A_{p2}/A_{p1}$, representing the damage induced to the prestressing steel area by corrosion phenomena, as specialized for the three considered case-studies.

For all the three case-study bridges, Fig. 11a confirms that, for the typical ranges of the numerical values of the parameters which characterize real existing post-tensioned elements, the prestressing force ratio ρ_P is roughly equal to the prestressing steel area ratio ρ, while Fig. 11b confirms that the cable stress ratio ρ_σ is almost equal to (or slightly larger than) 1.

For instance, considering $\rho = 0.8$ (20% of prestressing steel cross-section loss), on one hand for the post-tensioned girders characterized by low reinforcement ratios (examples 2 and 3), the prestressing force ratio is equal to $\rho_P = 0.81$ and the cable stress ratio is equal to $\rho_\sigma = 1.01$, meaning a 19% reduction in the prestressing force and a 1% increase in the cable stress. On the other hand, for the post-tensioned elements characterized by high reinforcement ratios (example 1), the prestressing

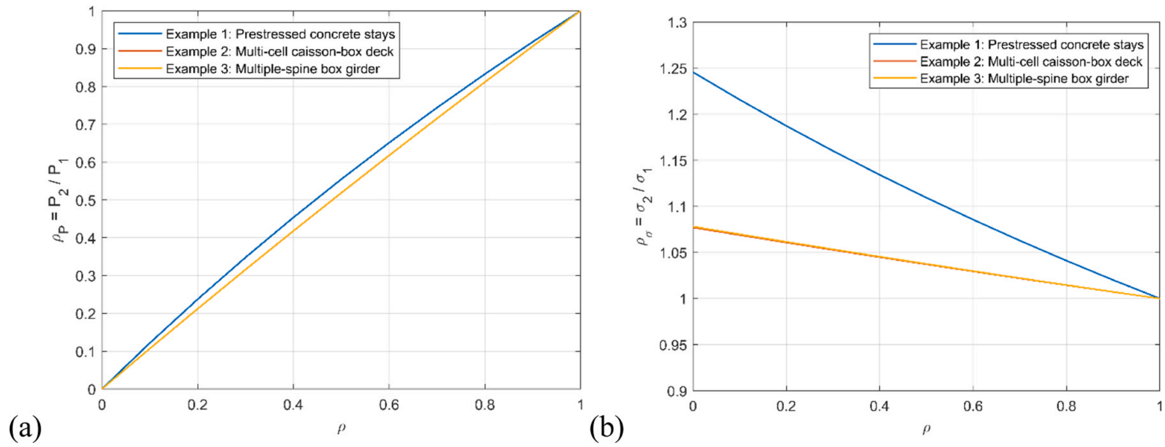

Fig. 11. Effects of corrosion for different values of prestressing steel area ratio: (a) effect on prestressing force; (b) effect on prestressing stress, for the considered bridge types.

force ratio is equal to $\rho_P = 0.83$ and the cable stress ratio is equal to $\rho_\sigma = 1.04$, meaning a 17% reduction in the prestressing force and a 4% increase in the cable stress. These numerical values indicate that prestressed stays are more susceptible than girders to cable stress increases due to corrosion (this may be due to the higher amount of prestressing steel area with respect to the concrete area). The analysis of real case-study bridges confirms the fundamental results of the theoretical formulation (basically: $\rho_P \cong \rho$ and $\rho_\sigma \cong 1$) for realistic ranges of the parameters.

Furthermore, since the initial prestress is commonly set as $\sigma_0 = 0.75 f_{pk}$, an increase of 25% in the prestressing steel stress could lead to stresses close to the yield strength of the prestressing steel. This leads to the conclusion that prestressed solutions characterized by high reinforcement ratios are more prone to reach a high stress state in the cables which could lead to the local failure of the tendon even if the structure is still substantially subjected to the same initial prestressing force P_1. On the contrary, bridge types with small reinforcement ratios could reach stress values in the cables that are lower than the ultimate or yielding value but still suffer from the reduction of the prestressing coactive state of the bridges that could lead to crack initiation or even failure of the damaged portion under the permanent loads.

6. Conclusions

This paper develops an analytical model to quantify the residual prestressing coactive state in post-tensioned concrete elements affected by lack of grouting and corrosion.

Reference is made to an equivalent cable, assuming uniform corrosion distribution and considering both concentric and eccentric tendons. The analytical formulation is developed for pre- and post-corrosion conditions by identifying three zones: a zone with lack of mortar injection where the prestressing cable can slide with respect to the concrete, a fully bonded zone, and a transition anchorage zone activated by variations in the coactive state. The model relies on a classical approach, based on equilibrium, compatibility, and linear elastic constitutive laws. The reduction of the prestressing steel area is assumed to induce both a loss of prestressing force and an increase of stress in the residual prestressing steel area, which are shown to occur simultaneously to ensure physical consistency. A sensitivity analysis with respect to the prestressing steel reinforcement ratio is performed, and the derived formulas are validated through comparison with experimental results available in the literature and numerical applications to existing prestressed concrete bridges, highlighting the practical implications of the proposed formulation.

The following fundamental and original results are obtained:

- Ready-to-use analytical formulas are provided for (I) the residual prestressing force and (II) the cable stress in the residual prestressing steel area, for the cases of both concentric and eccentric tendons.
- The reduction of the prestressing force acting in the zone characterized by lack of mortar injection is roughly equal to the reduction of the cable cross-sectional area due to corrosion. From a design and assessment points of view, this result is useful at the Serviceability Limit State.
- The stress in the residual prestressing steel area increases very slightly, reaching at most increases of + 25% for high values of prestressing reinforcement ratios (e.g. prestressed stays). In these cases, the effect of the cable stress increase may prove to be significant at the Ultimate Limit State. Indeed, an increase of 25% in the prestressing steel stress can lead to the total failure of the post-tensioned tendons since they are typically prestressed with initial stress values around 75% of their tensile rupture strength.
- The derived formulas are validated against experimental results available in the scientific literature, i.e., obtained for the specific case of external tendons for which the reinforcement ratios are approximately 50%.
- The fundamental result is that, for the typical values of the parameters, the loss of the prestressing force is predominant with respect to the (negligible) cable stress redistribution and it is approximately equal to (slightly larger than) the cross-section loss.
- The proposed formulas are intended as assessment tools, allowing designers to identify critical scenarios for both the Serviceability Limit States (e.g. deformability checks and stress verifications) and Ultimate Limit States (shear resistance capacity). In particular, the derived modification factors enable a direct update of the prestressing force and cable stress (P_2, σ_2), which can be incorporated into standard code-based verifications without modifying existing formulations [35,36]. The updated prestressing force directly affects the axial force and the average compressive stress in the concrete section (σ_{cp}), thereby influencing the shear resistance at ULS, while the updated cable stress is directly used in SLS stress limitation checks. Regarding flexural verification at ULS, only ρ is required, as the prestressing force is no longer active at this stage.

In conclusion, when combined with on-site inspections and/or monitoring systems, the analytical formulations developed in this study enable the quantification of the residual prestressing coactive state due to corrosion, supporting the service life prediction of post-tensioned elements.

CRediT authorship contribution statement

Matteo Marra: Writing – review & editing, Conceptualization. **Giada Gasparini:** Supervision, Methodology. **Emma Ghini:** Writing – original draft, Validation, Formal analysis, Conceptualization. **Stefano Silvestri:** Writing – review & editing, Validation, Supervision, Methodology, Conceptualization.

Funding

This research did not receive any specific grant from funding agencies in the public, commercial, or not-for-profit sectors.

Declaration of Competing Interest

The authors declare that they have no known competing financial interests or personal relationships that could have appeared to influence the work reported in this paper.

Acknowledgements

The authors are grateful to Prof. Maria Rosaria Pecce and Prof. Hugo Corres-Peiretti for the fruitful discussion that stimulated this research study.

Data Availability

All data, models, and codes generated or used during the study appear in the submitted article.

References

[1] Darmawan MS, Stewart MG. Spatial time-dependent reliability analysis of corroding pretensioned prestressed concrete bridge girders. Struct Saf 2007;29(1): 16–31.
[2] Lau K, Permeh S, Lasa I. Corrosion of prestress and posttension reinforced concrete bridges. Corrosion of steel in concrete structures. Elsevier; 2023. p. 81–105.
[3] Franceschini L, Belletti B, Tondolo F, Sanchez Montero J. A simplified stress–strain relationship for the mechanical behavior of corroded prestressing strands: The SCPS-model. Struct Concr 2022.
[4] Franceschini L, Vecchi F, Tondolo F, Belletti B, Sánchez Montero J. Mechanical behaviour of corroded strands under chloride attack: A new constitutive law. Constr Build Mater 2022;316:125872.
[5] Haskins R, White B, Ebeling R, Evans J. Relating corroded seven-strand, posttensioned cable cross-sectional properties to load capacity. J Eng 2016.
[6] Jeon CH, Lee JB, Shim CS. Tensile test of corroded strand and maintenance of corroded prestressed concrete girders. Int J Urban Civ Eng 2017;11(10):1384–8.
[7] Jeon CH, Lee JB, Lon S, Shim CS. Equivalent material model of corroded prestressing steel strand. J Mater Res Technol 2019;8(2):2450–60.
[8] Jeon CH, Nguyen CD, Shim CS. Assessment of mechanical properties of corroded prestressing strands. Appl Sci 2020;10(12):1–20.
[9] Lee BY, Koh KT, Ismail MA, Ryu HS, Kwon SJ. Corrosion and strength behaviors in prestressed tendon under various tensile stress and impressed current conditions. Adv Mater Sci Eng 2017.
[10] Lu ZH, Li F, Zhao YG. An investigation of degradation of mechanical behaviour of prestressing strands subjected to chloride attacking. Proc Int Conf Durab Concr Struct (ICDCS) 2016:57–65.
[11] Xu J, Chen W. Behavior of wires in parallel wire stayed cable under general corrosion effects. J Constr Steel Res 2013;85:40–7.
[12] Marra M. Strength and ductility of corroded strands within the framework of safety assessment of existing bridges. PhD thesis. University of Bologna. 2023.
[13] Marra M, Palermo M, Silvestri S, Trombetti T. On the influence of corrosion on the force-displacement behaviour of steel wires and strands. Proc Ital Concr Conf (ICC 2022) 2022:1–7.
[14] Marra M, Palermo M, Silvestri S, Trombetti T. Strength reduction curves for corroded seven-wire strands. Proc EUROSTRUCT23 2023:1–8.
[15] Recupero A, Spinella N, Tondolo F. A model for the analysis of ultimate capacity of RC and PC corroded beams. Adv Civ Eng 2018.
[16] Lu ZH, Zhou QH, Li H, Zhao YG. A new empirical model for residual flexural capacity of corroded post-tensioned prestressed concrete beams. Structures 2021; 34:4308–21.
[17] Recupero A, Spinella N. Experimental tests on corroded prestressed concrete beams subjected to transverse load. Struct Concr 2019;20:2220–9.
[18] Al-Mosawe D, Neves L, Owen J. Reliability analysis of deteriorated post-tensioned concrete bridges: The case study of Ynys-y-Gwas bridge in UK. Structures 2022;41: 242–59.
[19] MacDougall C, Bartlett FM. Mechanical model for unbonded seven-wire tendon with symmetric wire breaks. J Eng Mech 2005;131(12):1239–47.
[20] MacDougall C, Bartlett FM. Mechanical model for unbonded seven-wire tendon with single broken wire. J Eng Mech 2006;132(12):1345–53.
[21] Granata MF, Recupero A, Culotta G, Arici M. Influence of axial force and corrosion on failure of prestressed concrete structures considering M–V interaction. Eng Struct 2021;242:112552.
[22] De Domenico D, Messina D, Recupero A. A combined experimental–numerical framework for assessing the load-bearing capacity of existing PC bridge decks accounting for corrosion of prestressing strands. Materials 2021;14(17).
[23] Cestelli Guidi C. Cemento Armato Precompresso. Milano: Hoepli Ed.; 1987.
[24] Sprinkel MM. VDOT experience with grouts and grouted post-tensioned tendons. PTI J 2015.
[25] Santarella L. Il Cemento Armato. La Tecnica e la Statica. Milano: Hoepli Ed.; 1998.
[26] Walther R, Miehlbradt M. Progettare in Calcestruzzo Armato. Milano: Hoepli Ed.; 1994.
[27] Dai L, Chen Y, Wang L, Ma Y. Secondary anchorage and residual prestressing force in locally corroded PT beams after strand fracture. Constr Build Mater 2021;275: 122137.
[28] Lee JK, Kang JW. Experimental evaluation of vibration response of external post-tensioned tendons with corrosion. KSCE J Civ Eng 2019;23(6):2561–72.
[29] Wood SL, McKinstry CA, Lee JK. Residual tensile capacity of grouted post-tensioned tendons. Acids Struct J 2013;110(6):1099–107.
[30] Iori TL'. venzione di Morandi. SIXXI 5. Storia dell'ingegneria strutturale in Italia. Gangemi; 2020. p. 16–39.
[31] Nuti C, Briseghella B, Chen A, Lavorato D, Iori T, Vanzi I. Relevant outcomes from the history of Polcevera viaduct in Genova, from design to nowadays failure. J Civ Struct Health Monit 2020;10(1):87–107.
[32] Ghini E, Tomassetti L, Marra M, Silvestri S. Analytical study of cable corrosion effects due to lack of mortar injection in a post-tensioned concrete bridge. Proc fib Symp 2023:111–8.
[33] Marra M, Ghini E, Palermo M, Silvestri S. Effects of corrosion on the bending moment-curvature diagram of post-tensioned concrete elements. Proc fib Italy YMG Symp 2023:163–70.
[34] Furlanetto G. Il viadotto Stronetta presso Feriolo (Novara) per l'autostrada dei trafori. Ind Ital Cem 1990;646:664–79.
[35] CEN. EN 1992-1-1: Eurocode 2: Design of concrete structures - Part 1-1: General rules and rules for buildings. Brussels: European Committee for Standardization; 2004.
[36] NTC. *Norme tecniche per le costruzioni.* Decreto Ministeriale. 17/01/2018. Roma: Ministero delle Infrastrutture; 2018.
[37] fib. Model Code 2010 – Final draft, vol. 1. fib Bulletin No. 65. Lausanne; 2013..
[38] Ministero dei Lavori Pubblici. Norme tecniche per il calcolo, l'esecuzione ed il collaudo delle strutture in cemento armato normale e precompresso. Decreto Ministeriale 9 gennaio 1996. Roma. 1996.